Materials Research Bulletin 61 (2014) 306–314

Contents lists available at ScienceDirect

Materials Research Bulletin

journal homepage: www.elsevier.com/locate/matresbu

First principles treatment of structural, optical, and thermoelectric properties of Li_7MnN_4 as electrode for a Li secondary battery

Wilayat Khan [a,*], A.H. Reshak [a,b]

[a] New Technologies-Research Center, University of West Bohemia, Univerzitní 8, 306 14 Plzeň, Czech Republic
[b] Center of Excellence Geopolymer and Green Technology, School of Material Engineering, University Malaysia Perlis, 01007 Kangar, Perlis, Malaysia

ARTICLE INFO

Article history:
Received 5 April 2014
Received in revised form 22 September 2014
Accepted 5 October 2014
Available online xxx

Keywords:
A. Metal
D. Electronic structure
D. Optical properties
D. Thermal conductivity
Heat capacity
DFT

ABSTRACT

The electronic structure, electronic charge density and linear optical properties of the metallic Li_7MnN_4 compound, having cubic symmetry, are calculated using the full potential linearized augmented plane wave (FP-LAPW) method. The calculated band structure and density of states using the local density, generalized gradient and Engel–Vosko approximations, depict the metallic nature of the cubic Li_7MnN_4 compound. The bands crossing the Fermi level in the calculated band structure are mainly from the Mn-d states with small support of N-p states. In addition, the Mn-d states at the Fermi level enhance the density of states, which is very useful for the electronic transport properties. The valence electronic charge density depicts strong covalent bond between Mn and two N atoms and polar covalent bond between Mn and Li atoms. The frequency dependent linear optical properties like real and imaginary part of the dielectric function, optical conductivity, reflectivity and energy loss function are calculated on the basis of the computed band structure. Both intra-band and inter-band transitions contribute to the calculated optical parameters. Using the BoltzTraP code, the thermoelectric properties like electrical and thermal conductivity, Seebeck coefficient, power coefficient and heat capacity of the Li_7MnN_4 are also calculated as a function of temperature and studied.

1. Introduction

In recent years, researchers focused their attention on materials which will be useful to use for a Li secondary battery, in particular the studies of oxides, sulfides, and carbon materials. Despite the interest in these materials, in 1994 Nishijima et al. [1] have focused on lithium transition metal nitrides.

Lithium nitride Li_3N [2–8], is renowned due to its very high Li-ion conductivity at approximately 1×10^{-2} S/cm. However, this (Li_3N) possesses a small decomposition voltage (0.44 V) [9], which renders it too complex to be utilized as an electrolyte for a solid lithium battery.

It is recognized that numerous Li-p block-metal nitrides belonging to the general formula $Li_{2n-1}MN_n$ depict an anti-fluorite kind of symmetry [10]. In such materials, Li-ion resides in the position of fluorine in the CaF_2 compound. In materials like CaF_2, ZrQ, and pbF_2 with fluorite symmetries which are renowned as exceedingly anionic conductors, these nitrides, such $Li_{2n-1}MN_n$, create high Li-ion conductivity and greater stability. In this research area, there are numerous articles available on the nitrides, Li_3BN_2 [11,12], Li_3AlN_2 [13,14], Li_5SiN_3 [15,16], and so on, as solid lithium electrolytes.

In Li–Mn–N materials, in which M represents the position of a transition metal, which has also been recognized for a long period, for example, Li_5TiN_3 [17], Li_7VN_4 [18], $Li_{15}CrN_9$, Li_7MnN_4 [19], Li_3FeN_2 [20,21], etc. However, these materials have been investigated only for the purpose of their physical properties. The electron conduction of these compounds destroys their properties for an electrolyte. On the other hand, this weakness of the nitrides, $Li_{2n-1}MN_n$ (M = transition metal atoms), could be rendered a benefit if they are successful as an electrode for a Li secondary electric battery. The mutual uniqueness of high lithium ion mobility and the effortlessly changeable valence of the transition metal might ease the mixing and removal of Li in these nitrides.

Materials science has a great influence in several industrial fields by designing multifunctional materials. These materials have many applications in different industrial fields. A single material having many desirable properties can be suitable to meet the challenges. The promising multifunctional materials include transitional metal oxy-nitrides (TM–O–N). They are technologically important with applications in the fields of biocompatible coatings, solar absorbers, electrochromic coatings, nanocrystalline solar cells, and catalysts [22–25]. As compared to pure oxides, it has been discovered that TM–O–N compounds (TM = Ta, Hf, Zr, Ti)

* Corresponding author. Tel.: +420 775 526 684.
E-mail address: walayat76@gmail.com (W. Khan).

http://dx.doi.org/10.1016/j.materresbull.2014.10.021
0025-5408/

have improved optical properties [26]. Therefore, we thought it would be worthwhile to use the investigated compound (Li_7MnN_4), which is transitional metal nitrides, as a multifunctional material. Thus, we are interested in calculating the optical properties of Li_7MnN_4. Moreover, the investigation of the optical properties will help to reach a deep insight into the electronic structure. Therefore, we have studied the optical properties of the investigated compound.

It is well known that Li-ion batteries are very efficient devices for the storage of energy because of their greater energy density. In general, a Li-ion battery has high power density, which is decreased because of its high degree of polarization at greater rates of current. Investigation of the optical conductivity of Li cathode materials is essential to obtain a better understanding of the conduction phenomenon of ions, particularly used in Li-ion batteries [27]. The spectra of the energy loss function are used to introduce the plasmonic characteristic of the material.

Nishijima et al. [1] synthesize the above-mentioned nitrides by taking the reaction with transition metal nitride M_xN_y (M = Ti, V, Cr, Mn, and Fe) and Li nitride Li_3N. It has been observed that the preparation of Li_3FeN_2 and $LiTMnN_4$ is very easy on the basis of traditional ceramic techniques [1]. Nishijima et al. [1] also stated that Li^+ was easily removed from Li_3FeN_2, and used these nitrides as a successful compound in a Li secondary battery [28]. They also characterize the Li_7MnN_4 compound, and stated that this compound is a very efficient electrode for a Li secondary battery.

In the present work, we discuss the theoretical investigation to analyze the structural, electronic charge density and linear optical susceptibilities of Li_7MnN_4 using the full potential linearized augmented plane wave (FP-LAPW) method. Using the Boltzmann theory, the transport coefficients, like the Seebeck coefficient, electronic thermal, and electrical conductivity, the power factor and heat capacity are calculated with respect to temperature. These results indicate that this compound can be used for a thermoelectric application.

2. Computational method

In this article, the linear optical properties of Li_7MnN_4 are investigated with a self-consistent method to solve the Kohn–Sham equation on the basis of a full-potential linearized augmented plan wave (FP-LAPW), within the framework of density functional theory (DFT) [29,30], as incorporated in the WIEN2K code [31]. In the FP-LAPW method, the unit cell is split into an atomic sphere (MT) and an interstitial region (IR). We used the local density approximation (LDA) [32], the generalized gradient approximation (GGA) [33] and the Engel–Vosko generalized gradient approximation (EVGGA) [34] to solve the exchange correlation potential. For the convergence of energy eigenvalues, we used the $R_{MT}K_{MAX}$= 7 and 3000 k-points for the integration of the Brillouin zone (BZ). We performed our calculations using the experimental data of the Li_7MnN_4 compound [1]. The crystal structure is plotted in Fig. 1. We optimized the lattice parameter of the investigated compound using CA–LDA and PBE–GGA. The calculated lattice parameters found by using the PBE–GGA (9.5834) show close agreement with the experimental one (9.5453) in comparison to CA–LDA (9.4593).

3. Results and discussion

3.1. Electronic structure

The energy band structure calculation is very useful for analyzing most of the properties of the materials. Fig. 2(a–c), shows the band structure of the cubic Li_7MnN_4 compound along X, M, Γ, R, and X (the high symmetry points of the BZ). Using LDA, GGA, and EVGGA, we should emphasize that there is an insignificant difference between the three approximations. In addition, we investigated the total and projected density of states. Fig. 3(a–c) displays the calculated total density of states for the Li_7MnN_4 compound and the projected density of the states of Li, Mn, and N atoms. The total density of states is shifted toward higher energy when we move from LDA to GGA, then to EVGGA (Fig. 3a). From Fig. 3(b and c), it is obvious that the lower part of the partial density of states (PDOS) lies between −14.0 eV and −12.0 eV, and is mainly from N-s states with a minor contribution from the Li-s and Mn-p states. The s states of the Li atom, the s/p/d states of the Mn atom and the p states of the N atom also indicate some contribution to the second region of the PDOS from −5.06 eV to 0.0 eV (Fermi level), but the density of states corresponding to the Mn-d and N-p states are stronger than that of the Li-s and Mn-s/p states. The third part (lower part of the conduction band) mostly originates from the hybridization of Mn-d/p with N-p states. The last part ranging from 4.0 eV to 16.0 eV is formed by the entire states.

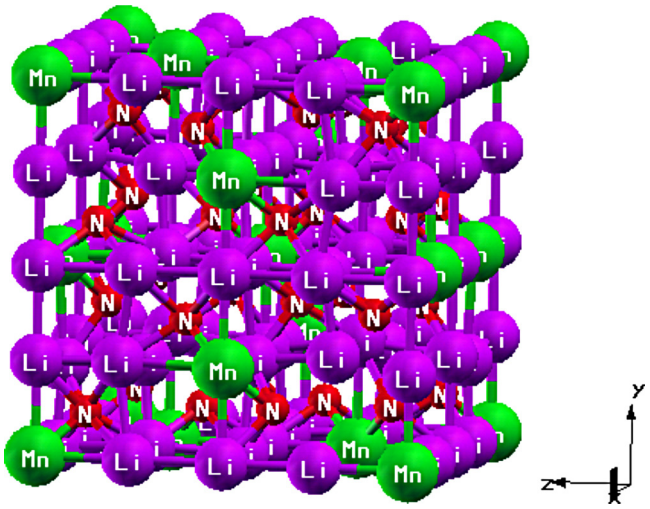

Fig. 1. Molecular structure of Li_7MnN_4.

Using LDA, GGA, and EVGGA, we have calculated the density of states $N(E_F)$ at Fermi level (E_F) as listed in Table 1. Knowing the values of $N(E_F)$, we also calculated the electronic specific heat capacity γ (see Table 1). The electronic specific heat coefficients γ for the investigated compound are calculated using the following relation taken from Refs. [35,36]:

$$\gamma = \frac{1}{3}\pi^2 N(E_F) K_\beta^2 \quad (1)$$

In the above relation, all the quantities in the right-hand side are constant, except $N(E_F)$, on which γ depends.

3.2. Electronic charge density

In order to investigate accurately the bonding nature and charge transfer from one atom to another, we have calculated the ground state valence electronic charge density of the investigated compound. The valence electronic charge densities are plotted along (1 1 0) and (1 0 0) crystallographic planes (Fig. 4). The electronegativity of Mn, Li, and N atoms are 1.83, 0.98, and 3.04, respectively. It is clear from Fig. 4a that there is a strong covalent bond between one Mn atom and two N atoms. The aim of calculating the electronic charge density in the (1 1 0) and (1 0 0) planes is to show the anisotropy between the two planes in a

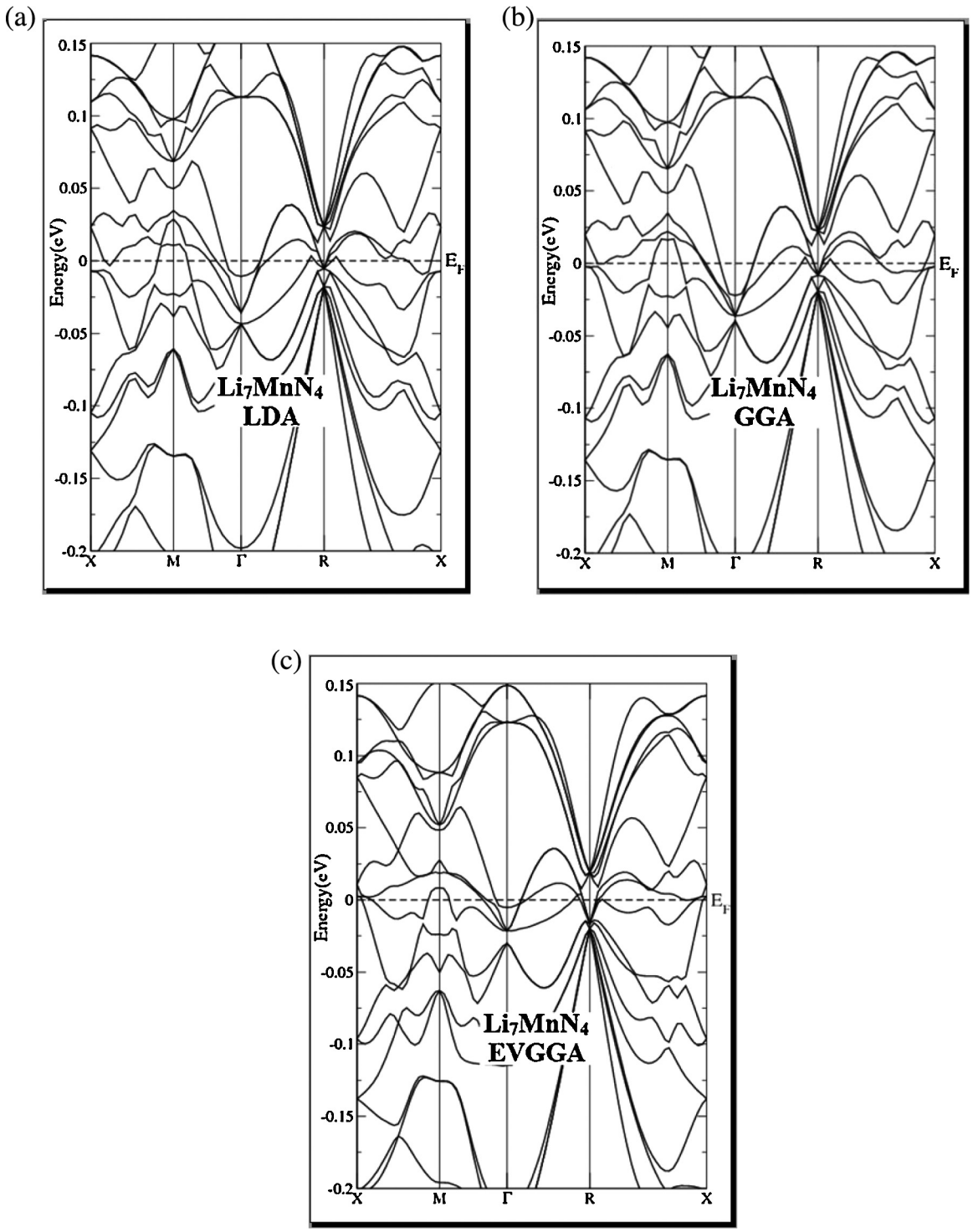

Fig. 2. Calculated band structure of Li_7MnN_4 using LDA, GGA, and EVGGA.

crystal. It is clear from Fig. 4b that the Li atom in the (1 0 0) plane shows no interaction with the Mn and N atoms. Due to the electronegativity difference (0.85) between Mn and Li atoms in the (1 0 0) crystallographic plane, the Mn atom shows a polar covalent bond with the Li atom. The thermo-scale presents the intensity of the electronic charge in which the blue color shows more charge while the red color shows zero charge density; therefore, the N atom has maximum charge density as compared to other atoms.

Our calculated bond lengths and bond angles of Li_7MnN_4 compound are listed in Tables 2 and 3. Our results indicate close agreement with the experimental data [1], which prove the accuracy of our calculations based on EVGGA exchange correlation potential.

3.3. Optical properties

In order to explain the linear optical properties of the investigated compound, we introduce the frequency dependent dielectric function i.e., $\varepsilon(\omega) = \varepsilon_1(\omega) + i\varepsilon_2(\omega)$. For the cubic crystal symmetry, the imaginary part $\varepsilon_2(\omega)$ of the complex dielectric

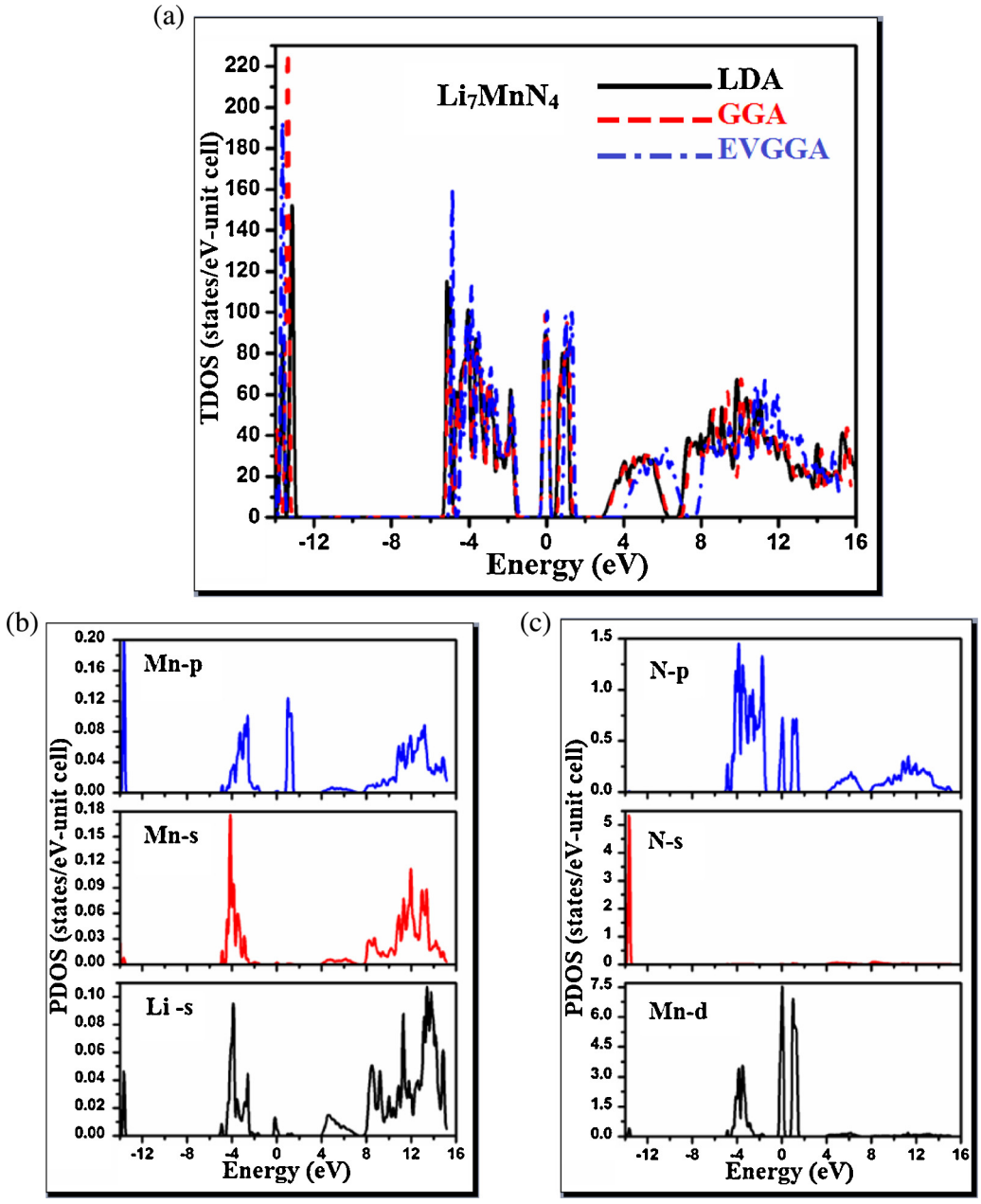

Fig. 3. Calculated total density state (TDOS) and partial density of states (PDOS) of the Li_7MnN_4 structure.

tensor is given by [37]:

$$\varepsilon_2(\omega) = \frac{8}{2\pi\omega^2}\sum |P_n k|^2 \frac{dS_k}{\nabla\omega_n(k)} \quad (2)$$

where the term $P_n k$ stands for the delocalized electron band transitions between initial and final states. It is found that there is a strong interrelationship between $\varepsilon_2(\omega)$ and the density of states. The real part $\varepsilon_1(\omega)$ can be obtained from the imaginary part $\varepsilon_2(\omega)$ of the dielectric function using the Kramers–Kronig transformation [38], as represented by the following expression:

$$\varepsilon_1(\omega) = \frac{2}{\pi}P\int_0^{\infty}\frac{\omega'\varepsilon_2(\omega)}{\omega'^2-\omega^2}d\omega \quad (3)$$

From the real and imaginary parts of the complex dielectric tensor, we can calculate the real and imaginary parts of the conductivity $\sigma(\omega)$, reflectivity $R(\omega)$, and energy loss function $L(\omega)$.

Fig. 5a shows the calculated imaginary part $\varepsilon_2(\omega)$ of the dielectric tensor for Li_7MnN_4. Since the investigated compound possesses a cubic structure, the linear optical properties are found to be isotropic. The imaginary part $\varepsilon_2(\omega)$ of the dielectric function corresponds to both inter-band and intra-band transitions. The sharp rise at low energy (>1.0 eV) is due to the intra-band

Table 1
Total density of states and electronic specific heat around the Fermi level of the Li_7MnN_4 compound.

Li_7 align="center"MnN4		
LDA	$N(E_F)$(states/eV)	γ (mJ/mol K^2)
GGA	95.9664	16.6477
EVGGA	92.0168	15.9626
	86.8908	15.0733

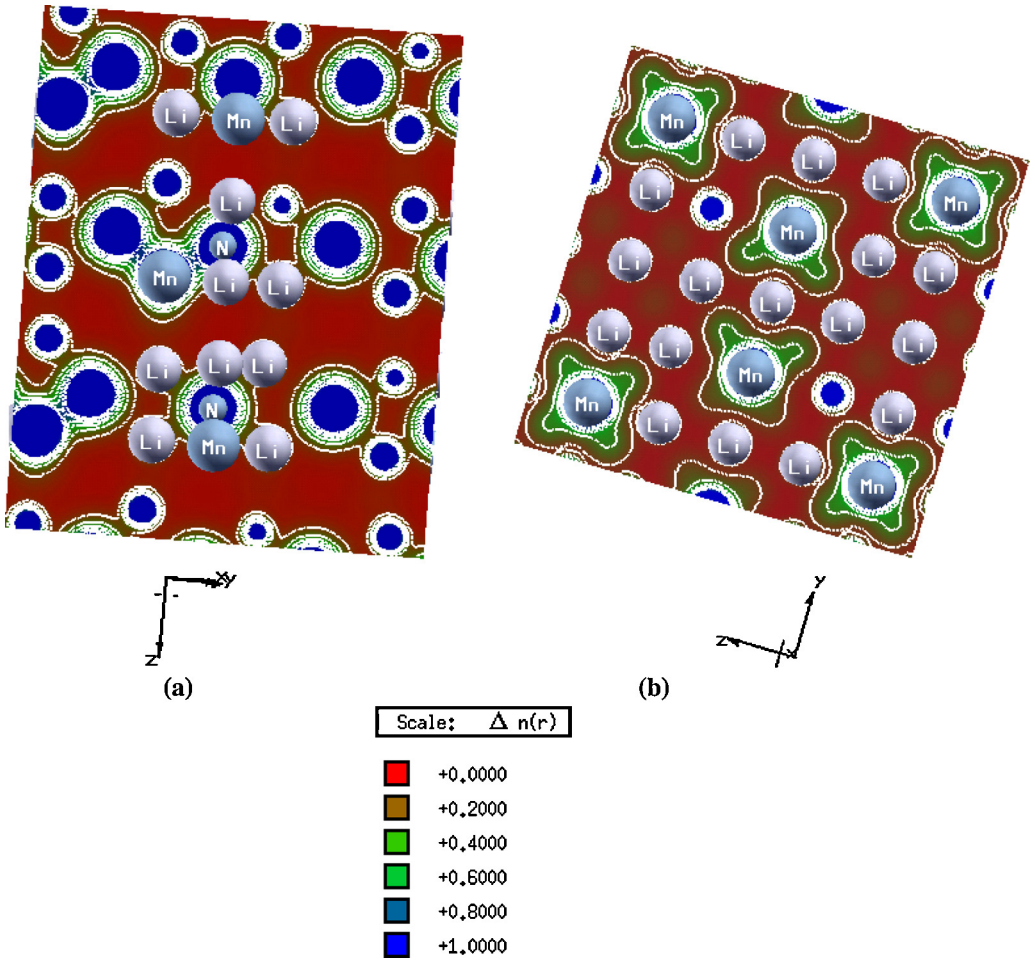

Fig. 4. Electronic space charge density distribution contour calculated with EVGGA in the (1 1 0) and (1 0 0) planes of Li_7MnN_4.

transition. The imaginary part $\varepsilon_2(\omega)$ of the dielectric tensor shows maximum peaks at 4.3 eV obtained due to the inter-band transitions of Mn-p states in the valence bands to N-p states of the conduction bands. The increase in energy of the incident photons above 5.8 eV results in a decrease in the spectral structure of $\varepsilon_2(\omega)$.

Fig. 5b shows the dispersion curve of the real part $\varepsilon_1(\omega)$ of the dielectric function. One can see that in the infrared range (IR), the intra-band absorption is governing; this is associated with the negative value of the real $\varepsilon_1(\omega)$ part of the complex dielectric tensor, which especially occur in the spectra of metallic compounds. The parameters which are used to find the intra-band absorption are (1) the conduction electrons and (2) plasma frequency (ω_p). It is also found that there is a direct proportionality between the square of the plasma frequency (ω_p^2) and the Fermi velocity (VF) (charge carrier) plus the concentration of free charge carriers N_{eff} [39].

The frequency-dependent real and imaginary parts of the optical conductivity $\sigma(\omega)$ are plotted in Fig. 5(c and d). The superposition of the inter/intra-band transition of electron results in better optical conductivity $\sigma(\omega)$ in metals. On the other hand, including the Drude term helps to present the optical conductivity $\sigma(\omega)$ in the IR range as shown in Fig. 5c. From Fig. 5c, it is clear that, above 0.7 eV, the peaks that appear in the optical conductivity $\sigma(\omega)$ spectra are due to the inter-band transition. The maximum value of the optical conductivity $\sigma(\omega) \sim 3.9 \times 10^{14} s^{-1}$ arises at 11.9 eV along the spectral region.

The calculated reflectivity $R(\omega)$ as a function of photon energy of Li_7MnN_4 is plotted in Fig. 5d. The compound shows maximum reflection in the low energy range, because the frequency of the incident photon cannot exceed the plasmon frequency $\left(\omega_p = (e^2 n/\varepsilon_0 m)^{1/2}\right)$ of the free electrons and emit the same

Table 2
Calculated and experimental bond lengths of the Li_7MnN_4 compound.

Li_7 align="center"MnN4		
Bond type	Bond lengths (calc)	Bond lengths (Exp)
N1-Li1	2.029	2.044
N1-Li2	2.126	2.030
N1-Li3	2.241	2.172
N1-Li4	2.155	2.163
N1-Li4	2.013	2.937
N1-Li5	2.170	2.225
N1-Li3	2.001	2.104
N1-Li4	2.229	2.095
N1-Li5	2.063	2.003
Mn1-N1	1.818	1.923
Mn2-N2	1.803	1.811

Table 3
Calculated and experimental bond angles of the Li_7MnN_4 compound.

Li_7 align="center"MnN4		
Bond type	Bond angles (calc)	Bond angles (Exp)
N1-Mn1-N1	108.46	110.8
N2-Mn2-N2	109.47	109.5

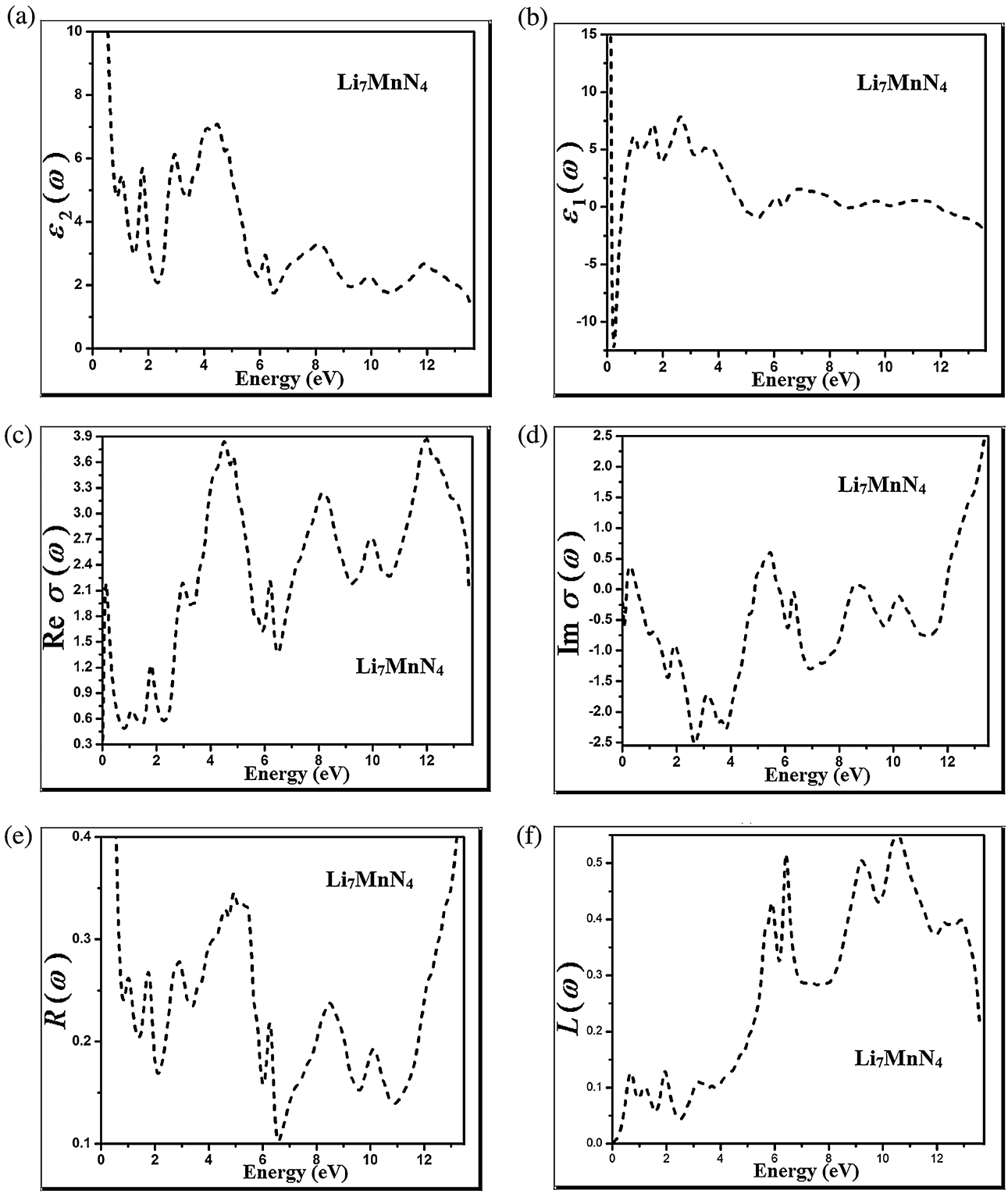

Fig. 5. Calculated real and imaginary parts of dielectric function, optical conductivity, reflectivity, and energy loss function of Li_7MnN_4 using EVGGA.

energy which is absorbed by the free electrons. The reflectivity spectrum shows fluctuation in the peaks in the energy range from 1.0 eV to 11.0 eV and in the energy range above 11.0 eV one can see the maximum value of the reflectivity.

Finally, from the frequency-dependent real and imaginary parts of the complex dielectric function, we calculate the energy loss function $L(\omega)$ in the energy range from 0.0 eV to 13.8 eV, as displayed in Fig. 5e. The energy loss function $L(\omega)$ increases with the photon energy ω and has two prominent peaks at energy 6.4 eV and 10.7 eV. Our calculated optical results emphasize that the electron–phonon interaction play principal role, which changing the optical properties [40].

3.4. Transport properties

From the band structure investigation, we calculate the electronic transport coefficients with constant relaxation time τ using the semi-classical Boltzmann theory as employed in the BoltzTraP computer package [41]. The electronic conductivity can be written as:

$$\sigma_{\alpha\beta}(\varepsilon) = \frac{e^2}{N}\sum_{i,k}\tau v_\alpha(i,k)\frac{\delta(\varepsilon-\varepsilon_{i,k})}{d\varepsilon} \quad (4)$$

where N number of selected k = points, τ = charge carriers constant scattering time, ε = band energy, α, β = indices of the tensor (transport coefficient), and the component of the group velocity ($v_\alpha(i,k)$) is proportional to the energy derivative ($d\varepsilon_{i,k}/dk_\alpha$).

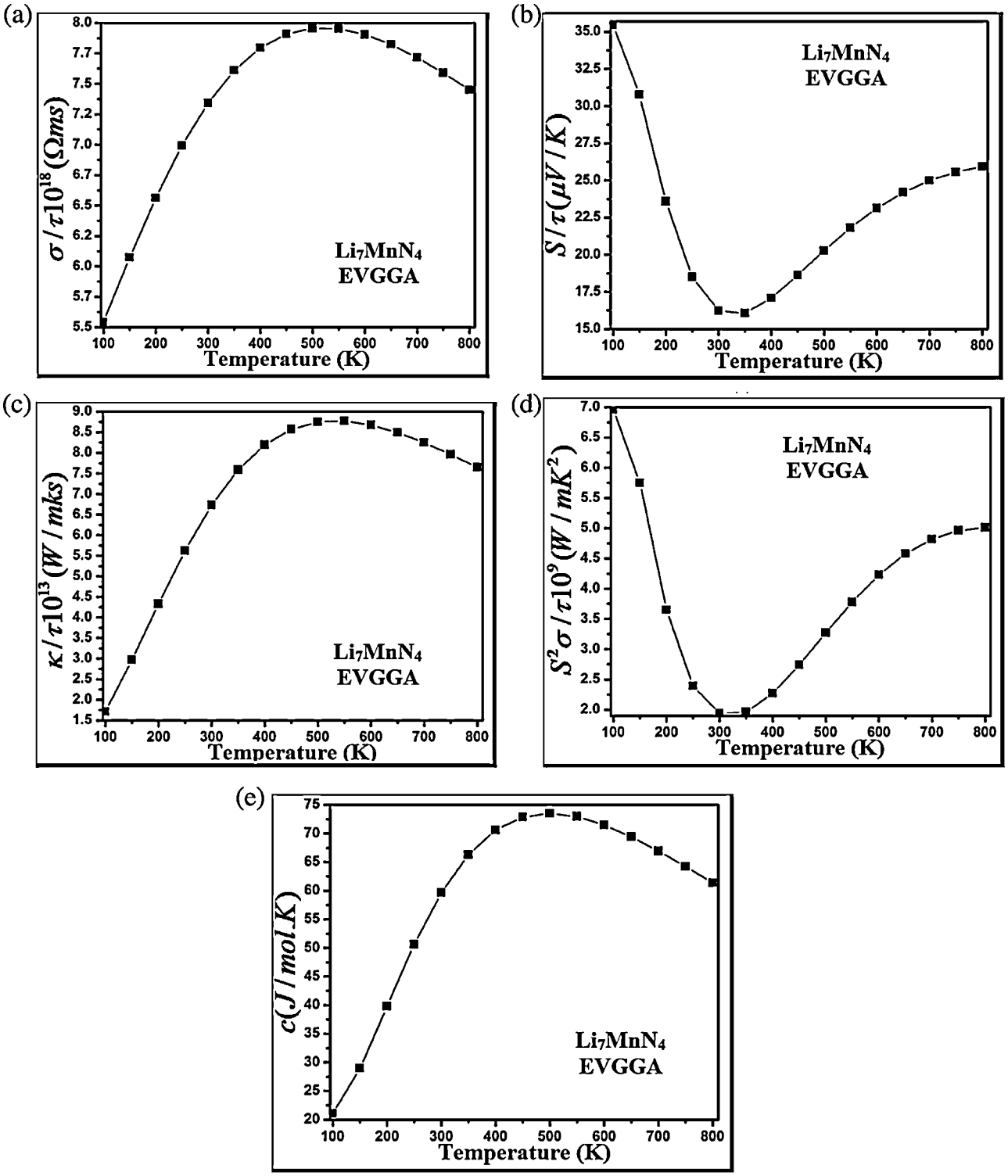

Fig. 6. Calculated transport coefficients of Li_7MnN_4 as a function of temperature: electrical conductivity, Seeback coefficient, thermal conductivity, power factor, and heat capacity.

The temperature and chemical potential dependent electronic transport coefficients can be calculated from the integration of transport distribution functions:

$$\sigma_{\alpha\beta}(T,\mu) = \frac{1}{\Omega}\int \sigma_{\alpha\beta}(\varepsilon)\left[-\frac{\partial f_\mu(T,\varepsilon)}{\partial\varepsilon}\right]d\varepsilon \quad (5)$$

$$S_{\alpha\beta} = \sum_\gamma (\sigma^{-1})_{\alpha\gamma}\nu_{\beta\gamma} \quad (6)$$

$$\nu_{\alpha\beta}(T,\mu) = \frac{1}{eT\Omega}\int \sigma_{\alpha\beta}(\varepsilon)(\varepsilon-\mu)\left[-\frac{\partial f_\mu(T,\varepsilon)}{\partial\varepsilon}\right]d\varepsilon \quad (7)$$

Here in the above equations,

f_μ = Fermi distribution function, μ = chemical potential (temperature dependent), T = temperature, and Ω = volume. The electronic thermal conductivity can be written as:

$$\kappa_{\alpha\beta}(T,\mu) = \frac{1}{e^2T\Omega}\int \sigma_{\alpha\beta}(\varepsilon)(\varepsilon-\mu)^2\left[-\frac{\partial f_\mu(T,\varepsilon)}{\partial\varepsilon}\right]d\varepsilon \quad (8)$$

This is an efficient technique for calculating the electronic transport properties of some known thermoelectric materials, which gives comparable results to the experimental data. Fig. 6a shows the variation of electrical conductivity (σ/τ) with temperature varying from 100 K to 800 K. The electrical conductivity (σ/τ) of the investigated compound Li_7MnN_4 increases due to the increase in temperature up to 500 K [42,43] and then starts decreasing when the temperature goes beyond 500 K. The main reason for the decrease in the electrical conductivity (σ/τ) with the increase in temperature is due to the charge carrier concentration increasing, for the reason that both thermally generated electrons and free electrons contribute to the conduction band, which enhance the electron–electron scattering and, as a result, reduces the mobility. Li_7MnN_4 indicates $5.5\times10^{18}(\Omega\,ms)$ at low temperature (100 K) and then reaches its maximum value of electrical conductivity, $7.9\times10^{18}(\Omega\,ms)$, at 500 K.

The Seebeck coefficient (S/τ) versus temperature is plotted in Fig. 6b. The Seebeck coefficient (S/τ) of Li_7MnN_4 is positive over the entire range of temperatures, which shows that the compound is a *P*-type doped material. The Seebeck coefficient (S/τ) of the compound presents the higher value 32.2 μV/K at 100 K and decreases linearly with temperature from 100 K to 350 K, because of the mixed conduction phenomenon. Beyond 350 K, (S/τ) increases exponentially with temperature and reaches its maximum value, 20.5 μV/K, and its saturation point at 800 K, as displayed in Fig. 6b. It is clear from Fig. 6b that increases in the temperature result in the enhancement of the hole doping in the Li_7MnN_4 compound.

Fig. 6c shows that the value of electronic thermal conductivity (κ_e/τ) of Li_7MnN_4 is very low $(1.75\times10^{13}(W/mks))$ at 100 K. It should be remembered that all the three components of the thermal conductivity are qualitatively equal i.e., $\kappa_a^{el} = \kappa_b^{el} = \kappa_c^{el}$, because the investigated compound is symmetrically cubic. Electronic thermal conductivity (κ_e) depicts a considerable contribution to the total conductivity (κ); we ignore the lattice thermal conductivity (κ_l) because it cannot be achieved from the band structure. Normally, using the Wiedemann–Franz law, one can estimate thermal conductivity (κ_e/τ) from electrical conductivity (σ), because both current as well as heat energy are carried by the free electrons. Fig. 6c shows that the thermal conductivity (κ_e/τ), after achieving the maximum value $8.75\times10^{13}(W/mks)$ at 550 K, gradually decreases with the increase in temperature beyond 550 K.

From the calculated Seebeck coefficient (S/τ) and electrical conductivity (σ/τ), we can find the power factor $(S^2\sigma)$. The electronic power factor $(S^2\sigma)$ of the relaxed *P*-type doped Li_7MnN_4 compound is reported in Fig. 6d, as a function of temperature ranging from 100 K to 800 K. The nature of the power factor $S^2\sigma$ is very similar to the thermo-power over the entire temperature range from 100 K to 800 K. The power factor $S^2\sigma$ increases monotonically with the increase in temperature from 350 K to 800 K. One can recognize from Fig. 6d that, due to the increase in temperature from 300 K, the power factor increases exponentially up to 700 K; beyond this temperature the power factor reaches its saturation. The maximum value of the calculated power factor $S^2\sigma$ is $5.0\times10^9(W/mK^2s)$ at 800 K (Fig. 6d).

The temperature-dependent electronic heat capacity $c_{el}(T_{el})$ of the Li_7MnO_4 compound is shown in Fig. 6e. Mathematically, the electronic specific heat capacity $c_{el}(T_{el})$ can be calculated as [44]:

$$c_{el}(T_{el}) = \int_{-\infty}^{\infty}\frac{\partial f(\varepsilon,\mu,T_{el})}{\partial T_{el}}g(\varepsilon)\varepsilon d\varepsilon \quad (9)$$

where $g(\varepsilon)$ density of states of electrons at E_F, μ = temperature T_{el}, and $f(\varepsilon,\mu,T_{el})$ = Fermi distribution function = $\left\{e^{\left[(\varepsilon-\mu)/k_BT_{el}\right]}+1\right\}^{-1}$. At low temperature, both Debye temperature θ_D and the density of states N_{el} at the Fermi level E_F is suitably estimated from the electronic specific heat. Here, we consider only the electronic contribution to the specific heat, because there is a linear relationship between the electronic specific heat and temperature, i.e. $c_{el}(T_{el})=\gamma T_{el}$, where γ = Sommerfeld co-efficient [45].

From Fig. 6e, one can see that the heat capacity increases with temperature up to 450 K. As the temperature of the electron system increases, empty states will become available below the Fermi level due to Fermi smearing. It is clear from Fig. 6e that the heat capacity of the investigated compound follows the Debye approximation (T^3), also called the anharmonic approximation [46].

Above 450 K, the heat capacity decreases with temperature and does not follow the experimental curve (Dulong–Petit limit) (Fig. 6e). From all the above discussion, we conclude that the investigated compound Li_7MnN_4 shows stability up to 800 K.

4. Conclusions

In this research study, we investigate the electronic structure and linear optical susceptibilities of the Li_7MnN_4 compound using the first principle calculation within density functional theory (DFT). The local density approach (LDA), generalized gradient approach (GGA) and Engel–Vosko generalized gradient approach (EVGGA) are used. We calculate the electronic band structure and density of states, which exhibit the metallic behavior of the investigated compound. Our calculated electronic charge density describes a strong covalent bond between Mn and N atoms, and a polar covalent bond between Li and Mn atoms. The electronic charge density contours also show that N atoms have maximum charge density than other atoms. We calculate the optical properties i.e., real and imaginary parts of the complex dielectric tensor, optical conductivity, reflectivity and energy loss function in terms of the electronic structure, and analyze that the optical properties are quite efficient in the UV region. The main peaks in the imaginary part $\varepsilon_2(\omega)$ of the dielectric tensor at energy of 4.3 eV are due to the inter-band transitions from the valence bands Mn-p states to the conduction bands N-p states. Our calculated optical conductivity shows maximum value $\sigma(\omega)\sim3.9\times10^{14}s^{-1}$ at energy 11.9 eV along the spectral region. The computed reflectivity of the investigated compound depicts 40% reflection at energy 13.8 eV, which depict that it is probable to be suitable electrical

conductor. We also calculate the thermoelectric properties i.e., electronic and thermal conductivity, Seebeck coefficient, power factor and heat capacity as a function of temperature within the framework of the BoltzTraP computer package. Our calculated power factor indicates that the title compound is suitable candidate for both cold devices as well as for thermal generation. The calculated heat capacity indicates good agreement with the Debye model and indicates the maximum value at 550 K.

Acknowledgements

This result was developed within the CENTEM project, reg. no. CZ.1.05/2.1.00/03.0088, co-funded by the ERDF as part of the Ministry of Education, Youth and Sports OP RDI program. MetaCentrum and the CERIT-SC under the program Centre CERIT Scientific Cloud, reg. no. CZ.1.05/3.2.00/08.0144.

References

[1] M. Nishijima, N. Tadokoro, Y. Takeda, N. Imanishi, O. Yamamoto, J. Electrochem. Soc. 141 (1994) 11.
[2] S. Knutz, B. Skaarup, Solid State Ionics 10 (1983) 371.
[3] P.M. Richards, J. Solid State Chem. 33 (1980) 127.
[4] R. Bittihn, Solid State Ionics 8 (1983) 83.
[5] M. Meyer, H. Rickert, U. Schwaitzer, Solid State Ionics 10 (1983) 689.
[6] M.E. Bell, A. Breitschwerdt, U. Alpen, Mater. Res. Bull. 16 (1981) 267.
[7] B.A. Boukamp, R.A. Huggins, Mater. Res. Bull. 13 (1978) 23.
[8] J.R. Rea, D.L. Foster, Mater. Res. Bull. 14 (1979) 841.
[9] A. Rabenau, Solid State Ionics 6 (1982) 277.
[10] R. Juza, K. Langer, V. Benda, Angew. Chem. 80 (1968) 373.
[11] H. Yamane, S. Kikkawa, M. Koizumi, Angew. Chem. 71 (1987) 1.
[12] S. Yamane, H. Horiguchi, M. Koizumi, J. Solid State Chem. 65 (1986) 6.
[13] H. Yamane, S. Kikkawa, M. Koizumi, Solid State Chem. 15 (1985) 51.
[14] R. Juza, F. Hund, Solid State Chem. 13 (1948) 257.
[15] H. Yamane, S. Kikkawa, M. Koizumi, Solid State Ionics 25 (1987) 183.
[16] R. Juza, H.H. Weber, E. Meyer-Simon, Z. Anorg. Allg. Chem. 48 (1953) 273.
[17] R. Juza, W. Gieren, J. Haug, Z. Anorg. Allg. Chem. 300 (1959) 61.
[18] S. Gudat, R. Kniep, A. Rabenau, Z. Naturforsch. 456 (1990) 111.
[19] R. Juza, E. Anschutz, H. Puff, Angew. Chem. 71 (1959) 161.
[20] M. Fromont, Rev. Chim. Miner. 4 (1967) 447.
[21] R. Gudat, A. Kniep, W. Bronger, U. Ruschewitz, J. Less-Common Met. 161 (1990) 31.
[22] T.I. Tsyganov, E. Maitz, E. Richter, H. Reuther, Surf. Coat. Tech. 200 (2005) 1041–1044.
[23] R. Mientus, R. Grotschel, K. Ellmer, Surf. Coat. Tech. 200 (2005) 341–345.
[24] M.A. Aegerter, Solar Energy Mater. Solar Cells 68 (2001) 401–422.
[25] W. Assmann, Th. Reichelt, T. Eisenhammer, A. Huber, H. Schellinger, R. Wolgemuth, Nucl. Instrum. Methods Phys. Res. B 113 (1996) 303–307.
[26] S. Venkataraj, D. Severin, S.H. Mohamed, J. Ngaruiya, O. Kappertz, M. Wuttig, Thin Solid Films 502 (2006) 228–234.
[27] Y. Jingwen, W. Feng, Q. Xinping, L. Ning, S. Yuefeng, Electrochim. Acta 56 (2011) 5587.
[28] N. Nishijima, Y. Takeda, O. Yamamoto, J. Solid State Chem. (2014) In press.
[29] P. Younbong, 7, 1997; 137-145.
[30] P. Hohenberg, W. Kohn, Phys. Rev. 136 (1964) 684.
[31] K. Balaha, G.K.H. Shewartz, D. Madsen, WIEN2K, An Augmented Plane Wave +Local Orbitals Program for Calculating Crystals Properties, Karlheinz Schewartz, Techn. Universitat, Wien, Austria, 2001 ISBN 3-9501031-1-2..
[32] J.P. Perdew, Y. Wang, Phys. Rev. B 45 (13) (1992) 244.
[33] J.P. Perdew, J.A. Chevary, S.H. Vosko, K.A. Jackson, M.R. Pederson, D.J. Singh, C. Fiolhais, Phys. Rev. B 46 (1992) 6671.
[34] E. Engel, S.H. Vosko, Phys. Rev. B 47 (1993) 13164;
E. Engel, S.H. Vosko, Phys. Rev. B 50 (1993) 10498.
[35] A.H. Reshak, S.A. Khan, J. Magn. Magn. Mater. 354 (2014) 216–221.
[36] A.H. Reshak, S. Azam, Int. J. Electrochem. Sci. 8 (2013) 10396–10423.
[37] S. Azam, A.H. Reshak, Phys. B. 431 (2013) 102–108.
[38] F. Wooten, Optical Properties of Solids Academic, New York, 1972.
[39] E. Shreder, S.V. Streltsov, A. Svyazhin, A. Makhnew, V.V. Marchenkov, A. Lukoyanov, H.W. Weber, J. Phys. Condens. Matter 20 (45) (2008) 212–219.
[40] M.I. Kolinko, J. Phys. Chem. Solids 53 (1992) 1315–1320.
[41] Georg K.H. Madsen, David J. Singh, Condens. Matter Mtrl. Sci. (2006) 8 February.
[42] K. Nouneh, I.V. Kityk, R. Viennois, S. Benet, S. Plucinski, Z. Golacki, S. Paschen, J. Phys. D: Appl. Phys. (UK) 38 (2005) 965–973.
[43] K. Nouneh, I.V. Kityk, R. Viennois, S. Benet, S. Charar, S. Malynych, S. Paschen, Mater. Lett. 61 (2007) 1142–1145.
[44] N.W. Ashcroft, N.D. Mermin, Solid State Phys. (Holt, Rinehart and Winston, New York) (1976) .
[45] Z. Zhang, Nano/Microscale Heat Transfer, McGraw-Hill, New York, 2007.
[46] Chen Dong et al. Chin. Phys. B, 1674–1056/2009/18(02)/0738–06.